Nuclear Instruments and Methods in Physics Research B xxx (2015) xxx–xxx

Contents lists available at ScienceDirect

Nuclear Instruments and Methods in Physics Research B

journal homepage: www.elsevier.com/locate/nimb

Progress in understanding heavy-ion stopping

P. Sigmund [a,*], A. Schinner [b]

[a] Department of Physics, Chemistry and Pharmacy, University of Southern Denmark, DK-5230 Odense M, Denmark
[b] Institut für Experimentalphysik, Johannes Kepler Universität, A-4040 Linz, Austria

ARTICLE INFO

Article history:
Received 2 November 2015
Received in revised form 20 December 2015
Accepted 21 December 2015
Available online xxxx

Keywords:
Stopping power
Swift heavy ions
Charge states
Reciprocity
Low-velocity stopping

ABSTRACT

We report some highlights of our work with heavy-ion stopping in the energy range where Bethe stopping theory breaks down. Main tools are our binary stopping theory (PASS code), the reciprocity principle, and Paul's data base. Comparisons are made between PASS and three alternative theoretical schemes (CasP, HISTOP and SLPA). In addition to equilibrium stopping we discuss frozen-charge stopping, deviations from linear velocity dependence below the Bragg peak, application of the reciprocity principle in low-velocity stopping, modeling of equilibrium charges, and the significance of the so-called effective charge.

1. Introduction

Research on the penetration of heavy ions in matter dates back to early studies of the scattering and stopping of fission fragments [1]. The subject received renewed interest with the application of accelerators in the study of atomic collisions and material properties [2,3], ion implantation [4], ion-beam modification [5], ion-beam analysis [6,7] and ion-beam therapy [8].

While the penetration of protons and alpha particles is well described by Bethe's [9] theory of the stopping of point charges over a wide range of beam energies, penetration theory for heavier particles increases in complexity with increasing atomic number Z_1 for several reasons:

- The Coulomb force is not necessarily a weak perturbation,
- The projectile cannot necessarily be treated as a point charge, and
- Energy may be lost in charge-changing collisions.

Fig. 1 shows a comparison of measured electronic stopping forces with well-known formulae by Bohr [10] and Bethe [9],

$$-\frac{dE}{dx}=\frac{4\pi Z_1^2 Z_2 e^4}{mv^2}NL;\quad L=\begin{cases}\ln\frac{2mv^2}{\hbar\omega} & \text{Bethe}\\ \ln\frac{Cmv^3}{Z_1e^2\omega} & \text{Bohr},\end{cases}\tag{1}$$

where Z_1, Z_2 are atomic numbers of the ion and the target, respectively, v the ion speed, ω is an effective resonance frequency of the target electrons, N the number of target atoms per volume, and $C=1.1229$. It is seen that within the energy range depicted in the graph, the Bohr formula comes closest to the experimental data down to ~0.5 MeV/u. This is consistent with the wellknown Bohr criterion [11],

$$\frac{2Z_1e^2}{\hbar v}\gtrsim 1\tag{2}$$

for the validity of a classical-orbit description of ion–electron scattering, the basis of Bohr's theory. The opposite limit, $Z_1e^2/\hbar v\lesssim 1$, is known to define the range of validity of the Born approximation, the basis of Bethe's theory [11].

Due to the logarithmic form of (1), both expressions drop below zero at some apparent threshold. This is an artifact of the mathematics involved, since energy is transferred from the ion to the target in both theories, and not in the reverse direction. For the Bohr theory this is easily repaired by avoiding asymptotic expansion in $1/v$ [12] (solid line). The same can be done for the Bethe formula, but whereas the solid line in Fig. 1 represents a universal result when plotted in appropriate units (L versus $mv^3/Z_1e^2\omega$), the corresponding result for the Bethe theory depends on the target and therefore has not been included.

Fig. 1 suggests that, over a wide energy range around the Bragg peak, Bohr theory should be a better starting point for understanding heavy-ion stopping than Bethe theory. This has led to a series of studies beginning with Ref. [14]. The present note summarizes some highlights of this development. The presentation is based

* Corresponding author.
E-mail address: sigmund@sdu.dk (P. Sigmund).

http://dx.doi.org/10.1016/j.nimb.2015.12.041
0168-583X/

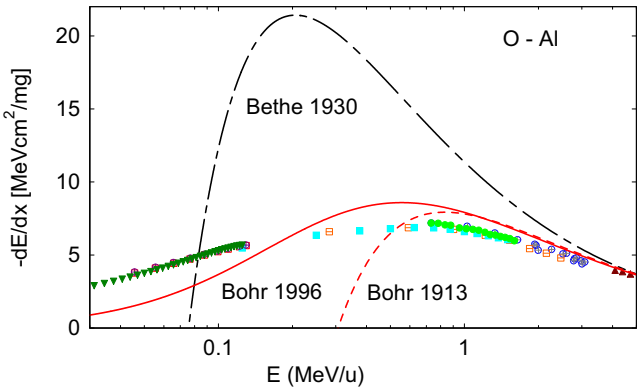

Fig. 1. Stopping force on oxygen ions in aluminum. Dashed line: Bohr formula [10]; Dot-dashed line: Bethe formula [9]; Solid line: Bohr theory avoiding asymptotic expansion [12]. Experimental data (symbols) compiled by Paul [13].

mainly on our own work, but comparisons with alternative theoretical schemes are made, and emphasis is laid on comparisons with experimental findings.

Although considerable progress has been made in straggling [15,16], the present paper focuses on mean energy loss.

2. Qualitative orientation

Bohr and Bethe stopping theory, as expressed by (1), ignore several important physical phenomena,

- *Screening of the Coulomb interaction* by electrons bound to the projectile. According to Bohr [1], electrons with orbital speeds v_e less than the projectile speed v tend to be stripped. Since both Bohr and Bethe theory consider the projectile as a point charge, a screening correction must be expected for

$$v \lesssim v_0 Z_1^{2/3}, \tag{3}$$

  where we characterize projectile electrons by their Thomas–Fermi speed $v_{\mathrm{TF}} = v_0 Z_1^{2/3}$, v_0 denoting the Bohr speed.
- *Orbital motion of target electrons* is ignored in Bohr theory. Although this effect (shell correction), is inherent in Bethe theory, its contribution to the stopping cross section is not taken into account in the asymptotic formula (1). Such a correction must be expected for

$$v \lesssim v_0 Z_2^{2/3}, \tag{4}$$

  where the Thomas–Fermi speed $v_0 Z_2^{2/3}$ characterizes the target atom.

Thus, if v decreases from the high-speed limit where (1) applies, screening will be the dominating correction to be taken into account if $Z_1 \gg Z_2$, while the shell correction will dominate for $Z_1 \ll Z_2$.

Consider now a situation where projectile screening is important, i.e., (3) applies. Then the Bohr parameter (2)

$$\frac{2Z_1 e^2}{\hbar v} \gtrsim \frac{2Z_1 e^2}{\hbar v_0 Z_1^{2/3}} = 2Z_1^{1/3} \tag{5}$$

will be greater than 1 for all values of Z_1. Therefore, in the presence of substantial projectile screening, the Born approximation, and hence Bethe theory, cannot be expected to provide a valid theoretical basis. This finding, emphasized by Bohr in 1948 [11], has been ignored in numerous theoretical studies over half a century.

- Another important effect, studied primarily in light-ion stopping, is *charge asymmetry* or *Barkas–Andersen effect*, characterized by the factor [17,18]

$$\frac{Z_1 e^2 \omega}{m v^3}. \tag{6}$$

If we approximate $\hbar\omega \sim Z_2 m v_0^2/2$ according to Bloch [19], we find that charge asymmetry becomes important for

$$v \lesssim (Z_1 Z_2/2)^{1/3} v_0, \tag{7}$$

indicating that this correction is intermediate between screening and shell correction, (3) and (4), respectively.

3. Theoretical schemes

Table 1 lists theoretical schemes which have been developed to estimate stopping cross sections for heavy ions in cold matter.[1] As noted in the last column, three of the listed schemes are high-speed theories incorporating effects that extend the range of validity towards lower velocities. The opposite holds for the scheme listed in the third row.

All these schemes incorporate features that are not taken into account in Bethe or Bohr stopping theory. While not ab initio theories, none of them employs adjustable parameters fitted to measured or tabulated stopping forces. Moreover, none of them make use of the (still) popular effective-charge concept. A brief discussion of the inadequacy of this type of description, based on Ref. [24], has been included in an Appendix A.

Table 2 lists effects entering the various schemes:

- Binding forces on target electrons enter explicitly into binary theory and PCA/UCA (Perturbed convolution approximation/Unitary convolution approximation) but not into the free-electron model TCS-EFRS (Transport cross section-extended Friedel sum rule). In SLPA (Shellwise local plasma approximation) the effect is taken into account implicitly via a local-density approximation (LDA).
- All models allow for orbital motion of target electrons (shell correction), static screening of the projectile by bound electrons, and variation of the ion charge.
- Charge asymmetry (Barkas–Andersen effect) is inherent in all schemes, although the case of CasP is special, as will be discussed below.
- Projectile excitation enters PASS and SLPA. In CasP, projectile excitation can be computed but is not part of the default option.
- Charge exchange is included in CasP, although not in the default version. Binary theory incorporates an estimate requiring charge equilibrium.
- Only the CasP code is available on the internet.

There are significant differences in the way how the above effects are treated in these theoretical schemes. Some of those aspects have been discussed in Ref. [25], but for details we refer to the original papers and various followups.

Fig. 2 shows a comparison of measured stopping cross sections with predictions of PASS and CasP for the O–Al system. This ion-target combination is exceptionally well covered with experimental data in good mutual agreement over an energy interval of six orders of magnitude. While the agreement with PASS data is close to perfect, CasP data lie below experiment from ~1 MeV/u down. The Bohr speed v_0 has been marked to emphasize the fact that neither PASS nor CasP can be expected to cover lower velocities. The

[1] The term 'cold matter' is meant to indicate that high-temperature-plasma targets require separate consideration.

Please cite this article in press as: P. Sigmund, A. Schinner, Progress in understanding heavy-ion stopping, Nucl. Instr. Meth. B (2015), http://dx.doi.org/10.1016/j.nimb.2015.12.041

Table 1
Theoretical schemes covering a wide energy range.

Scheme	Refs.	Code	Target	Starting at	Domain
Binary theory	[20]	PASS	Atom	Bohr	High v downward
PCA/UCA	[21]	CasP	Atom	Bethe-Bloch	High v downward
TCS-EFSR	[22]	HISTOP	Fermi gas	Quantal	Low v upward
SLPA	[23]		LDA	Quantal	High v downward

Table 2
Incorporation of effects affecting stopping cross sections. For the meaning of the brackets see text.

Effect	PASS	CasP	TCS-EFSR	SLPA
Atomic binding	Yes	Yes	No	(Yes)
Orbital motion (target)	Yes	Yes	Yes	Yes
Static screening	Yes	Yes	Yes	Yes
Variable charge	Yes	Yes	Yes	Yes
Charge asymmetry	Yes	(Yes)	Yes	Yes
Projectile excitation	Yes	(Yes)	No	Yes
Charge exchange	(Yes)	(Yes)	No	No
Code on internet	No	Yes	No	No

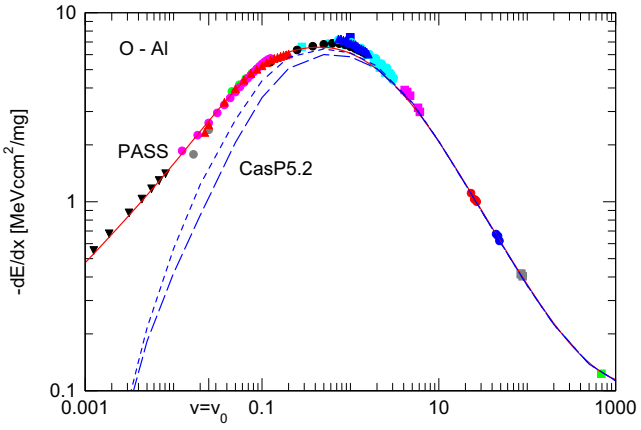

Fig. 2. Stopping force on oxygen in aluminum. Symbols: Experimental data extracted from Ref. [13]. Solid red line: PASS. Blue lines: CasP5.2 (dashed: default, dotted: including electron loss and capture). From [26], amended by the predictions of CasP. (For interpretation of the references to color in this figure legend, the reader is referred to the web version of this article.)

good agreement found for $v < v_0$ of PASS data is not a general feature, as will be seen below.

Fig. 3 shows an attempt to identify possible reasons for the discrepancy between the predictions in Fig. 2. For clarity, only target excitation/ionization is considered. Therefore experimental data have not been included. The four PASS curves confirm that the shell correction exceeds the Barkas–Andersen term, as it must be according to Section 2. Although both shell and Barkas–Andersen corrections are included in the CasP5.2 curve, this curve is quite close to the PASS curve 'No shell, no Barkas' which ignores both effects. We note that Barkas–Andersen corrections in CasP are taken over from PASS, although not shell-corrected.[2] Altogether we assert that the difference must originate primarily in the applied shell corrections.

Fig. 4 shows a comparison for the N–Ar system. The coverage with experimental data is smaller here, and the scatter between

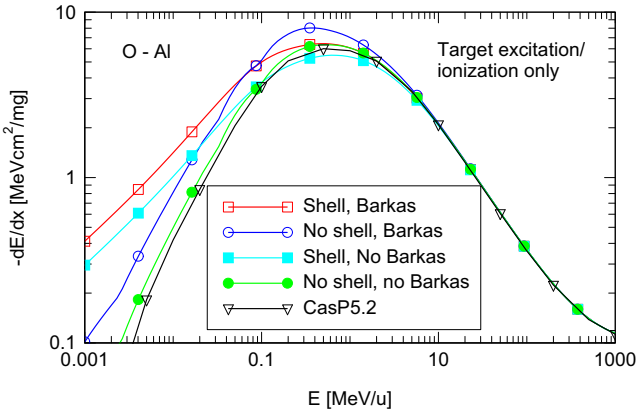

Fig. 3. Stopping force on oxygen in aluminum: charge exchange and projectile excitation/ionization neglected. PASS calculations with Barkas–Andersen and shell correction turned on or off (see legend). CasP5.2 default option including Barkas–Andersen and shell correction.

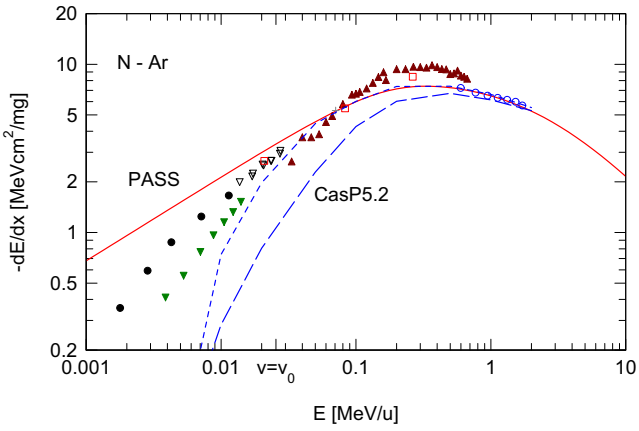

Fig. 4. Same as Fig. 2 for nitrogen in argon.

data from different sources is substantial. The difference between experimental and CasP data is greater than for O–Al, and also PASS data deviate noticeably from measurements, in particular in the velocity range below v_0.

Fig. 5 shows comparisons between PASS and SLPA [23,27] data and measured stopping cross sections in Zn. With the exception of He–Zn, where experimental data scatter substantially at the low-energy end, differences between PASS and SLPA as well as between experiment and the two theoretical schemes are below ~20%. SLPA data are in slightly better agreement with experiment for ions up to B. Quite good agreement is found for C ions in both schemes, whereas PASS data seem to better describe the measurements with O and Ag ions.

4. Frozen-charge stopping

As mentioned in Table 2, all theoretical schemes allow to estimate the dependence of the stopping cross section on the ion charge. Only few measurements have been reported on 'frozen charge' stopping, cf. [29–31] and followups. An example is shown in Fig. 6. There is found near-complete agreement between PASS and CasP output and reasonable agreement with experimental data from Ref. [28]. The beam energy, 10.59 MeV/u, lies in the regime of weak screening, where the Born approximation represents an appropriate starting point. Similar agreement has been achieved at energies within the classical regime [25].

[2] Private communication by P. L. Grande.

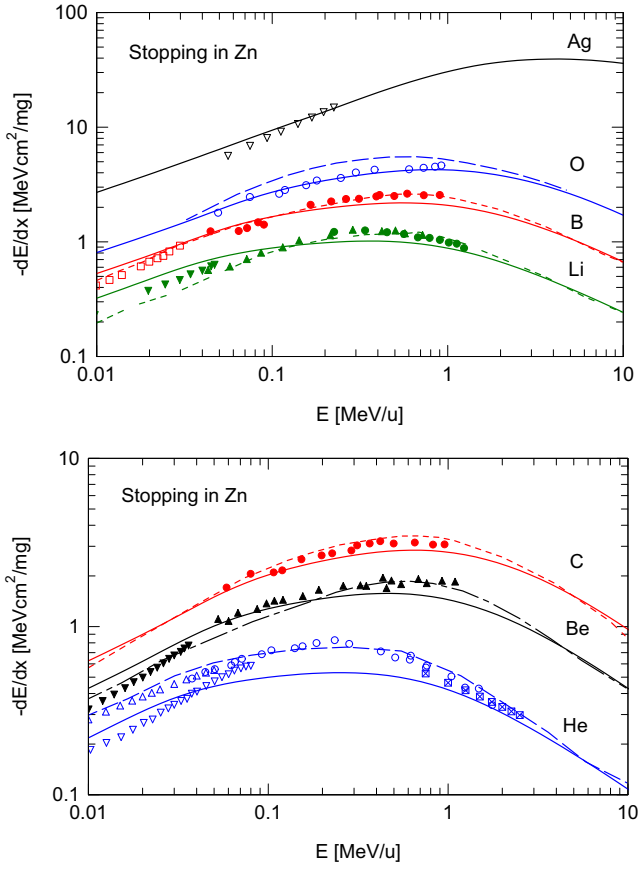

Fig. 5. Stopping forces on Ag, O, B and Li ions (upper graph) and C, Be and He (lower graph) in zinc. Solid lines: PASS results. Broken lines: SLPA. Data points extracted from Ref. [13].

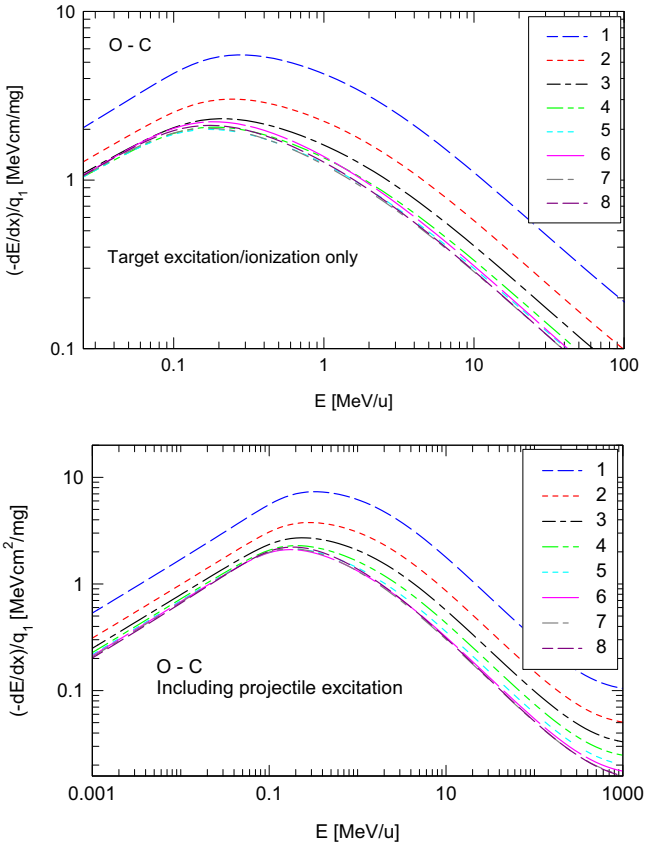

Fig. 7. Stopping force on O ions in C versus beam energy for charge numbers 1–8, calculated by PASS. Plotted is the ratio of $-dE/dx$ and the charge number q_1. Upper graph: target excitation/ionization only. Lower graph: Including projectile excitation.

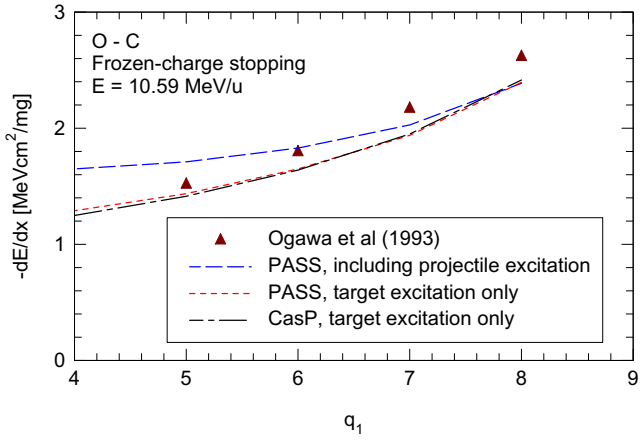

Fig. 6. Frozen-charge stopping forces versus charge number q_1 for O in C. Experimental data from Ref. [28]. Calculations from PASS and CasP code.

On the basis of the Z_1^2-dependence of the Bethe formula (1) it has been almost universally assumed that the frozen-charge stopping cross section would be proportional to the square of the ion charge q_1. Fig. 7 shows frozen-charge stopping forces for O ions in C calculated by PASS, divided by the charge number q_1 of the ion. It is seen that for charge states $q_1 = 5$–8 the stopping force is practically proportional to q_1 for all beam energies considered, regardless of whether or not projectile excitation is included in the calculations. If only target excitation is considered, this scaling property includes $q_1 = 4$. Similar trends have been found for other ion-target combinations [25].

A q_1^2 dependence of the stopping cross section cannot be expected in the classical regime, as is evident from the occurrence of Z_1 in the Bohr stopping formula (1). Fig. 8, upper graph shows that such a dependence is not predicted either by the Born approximation. Broken lines reflect Bethe stopping theory applied to screened ions [32]. Solid lines were evaluated by multiplying the straight Bethe formula for O–C by $(q_1/Z_1)^2$, as has been widely assumed in the literature. Pronounced differences are seen over the entire energy range covered in the graph. The graph reveals that asymptotically at high v, the difference amounts to ~20% for O^{6+}, a factor of two for O^{4+} and an order of magnitude for O^{2+}.

The lower graph in Fig. 8 shows a comparison between PASS output and the Born curves shown in the upper graph. Corresponding curves agree at high velocities, since binary theory approaches the Bethe limit thanks to an inverse-Bloch correction [26]. The main conclusion from this graph is that the transition from the classical to the Born regime takes place in approximately the same velocity regime for all charge states. This is in striking contrast with Northcliffe's assumption [33] that Z_1 in Bohr's criterion 2 should be replaced by q_1 for a screened ion.

5. Below the Bragg peak

Lindhard and Scharff [36] asserted electronic stopping cross sections for heavy ions to be proportional to v at speeds up to $\sim v_{TF} = v_0 Z_1^{2/3}$. This was shown to be confirmed by range

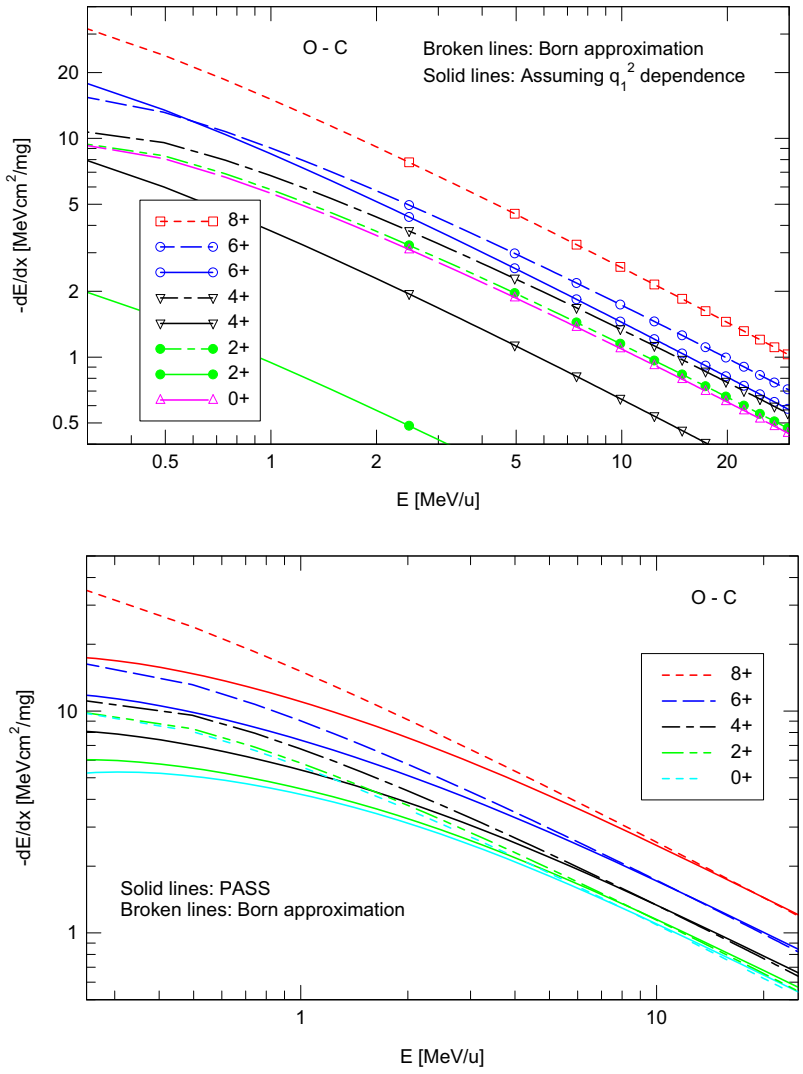

Fig. 8. Frozen-charge stopping for O in C. Only target excitation/ionization considered. Upper graph: stopping force from Born approximation (broken lines). Solid lines: assuming q_1^2-dependent stopping. Lower graph: comparison between PASS output (solid line) and results from Born approximation (dashed lines).

measurements with fission fragments [37]. However, two studies in 1966 showed that this assertion was only approximately correct:

1. Fastrup et al. [38] could match experimental results[3] with several ions on carbon at $v \lesssim v_0$ by a relation $S \propto E^p$, where the coefficient p in several cases differed substantially from $p = 1/2$.
2. Moak and Brown [39,40] found, for heavy ions like bromine and iodine at $v > v_0$, a linear velocity dependence but with an apparent threshold.

The second finding was taken up recently by Lifschitz and Arista [34]. On the basis of calculations on Br–C by their TCS-EFSR scheme, shown as the green solid line in Fig. 9, they concluded that the stopping cross section goes as $\propto v$ at velocities below the range covered by the measurements of Brown and Moak, and instead of a threshold they found a sudden change in slope.

Fig. 9 illustrates the case of Br in C by including experimental data from [41–43] as well as calculations from [34] and by PASS. In accordance with Ref. [34] we conclude that instead of an apparent threshold there is a positive curvature. This is found up to a velocity $\sim 0.4 v_{TF}$, where the stopping force bends off toward the Bragg peak. The positive curvature is substantial, as is evident from the stippled line which is an extrapolation of the low-speed

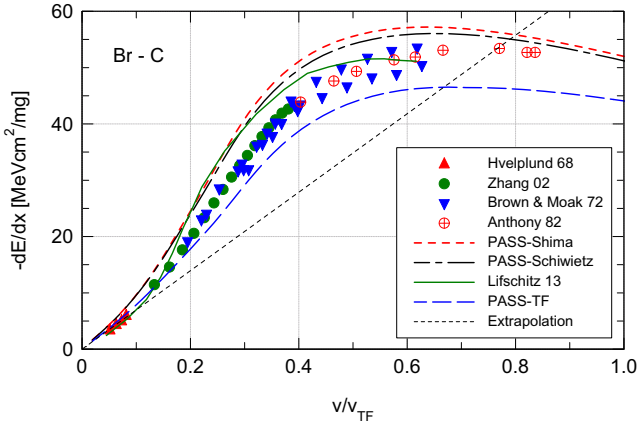

Fig. 9. Stopping of Br in C: experimental data from [13]. Calculations from [34,35]. See text. From [35].

[3] Throughout this paper we deal with electronic stopping. Experimental data in the velocity range below the Bragg peak typically need to be corrected for nuclear stopping. In the following, the symbol S denotes the electronic stopping cross section.

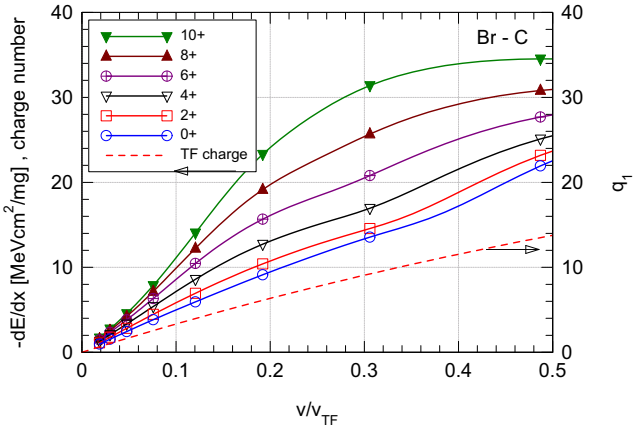

Fig. 10. Frozen-charge stopping force for Br–C calculated by PASS. Also included is the mean equilibrium charge according to (8). From [35].

behavior. PASS calculations have been performed with what we call the standard Thomas–Fermi charge

$$q_1 = Z_1\left(1 - e^{-v/v_{TF}}\right) \tag{8}$$

as well as expressions proposed by Shima et al. [44] and Schiwietz and Grande [45]. It is seen that experimental points lie between the Thomas–Fermi and the Schiwietz curves, in fact somewhat closer to the former, while the curve by Lifschitz and Arista overestimates the sudden change in slope.

Stimulated by the work of Lifschitz and Arista [34] we have studied the behavior of the stopping cross section below the Bragg peak [35]. By plotting numerous measured stopping cross sections tabulated in Ref. [13] and performing calculations by PASS we found that

- Dependent on the ion-target combination, both positive and negative curvature may be found in the considered velocity range,
- Stopping cross sections for heavy ions, separated into contributions from different target shells, exhibit positive curvature,
- Stopping by projectile excitation tends to produce negative curvature,
- Positive curvature is mainly due to increasing contribution from higher charge states.

In support of the dominating role of the charge states we mention that measured stopping cross sections for protons do not show positive curvature. Moreover, if the stopping cross section for a heavy ion is written as $S(v, q_1)$, where $q_1(v)e$ is the mean ion charge, a positive curvature implies that

$$\frac{dS(v,q_1)}{dv} = \frac{\partial S(v,q_1)}{\partial v} + \frac{\partial S(v,q_1)}{\partial q_1}\frac{dq_1(v)}{dv} \tag{9}$$

must increase with increasing v.

Fig. 10 shows frozen-charge stopping forces for Br–C according to PASS. Contributions to (9) were evaluated and plotted in Fig. 11. It is seen that the second term in (9), characterizing the effect of increasing ion charge, is monotonically increasing up to ~0.3, whereafter it is slowly decreasing. The first term, on the other hand, increases slightly up to $v/v_{TF} \sim 0.1$, whereafter it decreases slowly. This is opposite to the sudden rise found in Ref. [34] at $v/v_{TF} \sim 0.1$.

6. Low-velocity stopping

The literature on stopping of ions in the velocity range up to the Bohr speed is quite substantial, both on the experimental and the theoretical side [13,25,46]. Experimental problems arise from the need to separate electronic from nuclear stopping – where the latter may well be the dominating effect – and the need for very thin target foils. As regards theory there is missing a comprehensive scheme with a complexity somewhere between the classics of Firsov [47] and Lindhard & Scharff [36] on the one hand and brute-force ab initio calculations for individual ion-target combinations on the other.

A critical test of any low-velocity theory is its ability to reproduce Z_1 structure in the stopping cross section for a given material. While modified Firsov or Lindhard theories [25] tend to predict less pronounced structure than found experimentally, the opposite is found for more recent electron–gas calculations [22,48], although there are successes in a small number of cases such as stopping in the ⟨1 1 0⟩ direction of silicon crystals [48].

In the absence of a comprehensive scheme, application of the reciprocity principle [49] may be of some use: Consider a collision between two gas atoms 1 and 2 resulting in an energy loss $Q(v,p)$ that will depend on the impact parameter p. This results in an inelastic energy-loss cross section

$$S(v) = \int 2\pi p\, dp\, Q(v,p). \tag{10}$$

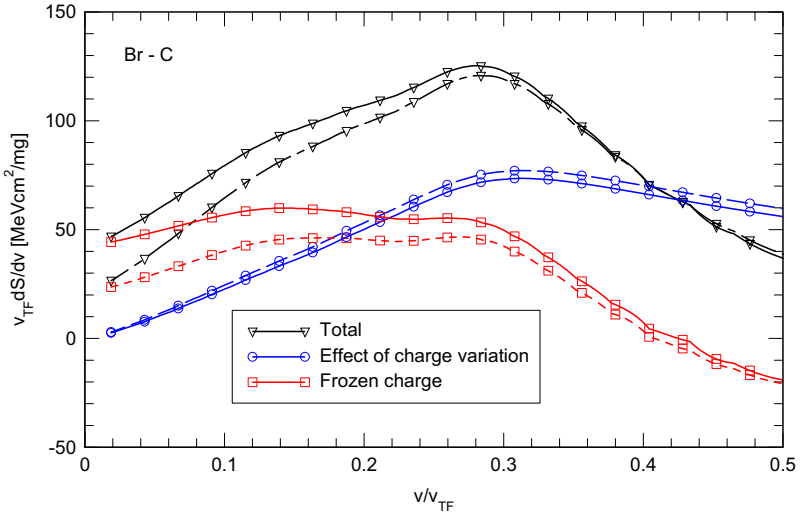

Fig. 11. Contributions to (9) for Br–C calculated by PASS. Solid lines: target and projectile excitation. Broken lines: target excitation only.

Please cite this article in press as: P. Sigmund, A. Schinner, Progress in understanding heavy-ion stopping, Nucl. Instr. Meth. B (2015), http://dx.doi.org/10.1016/j.nimb.2015.12.041

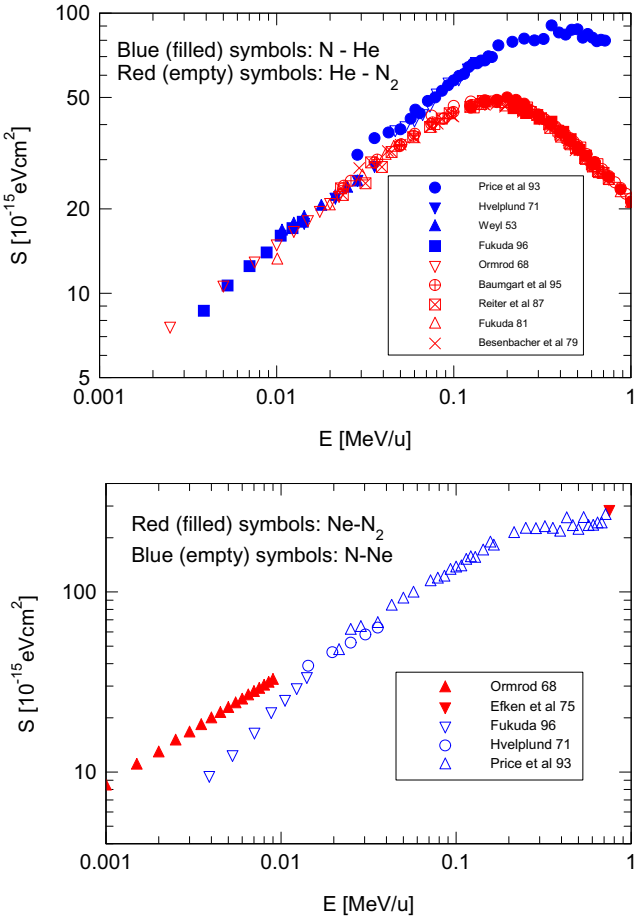

Fig. 12. Reciprocity for low-energy stopping in gas targets. Upper graph: He–N_2 and N–He. Lower graph: Ne–N_2 and N–Ne. Experimental data compiled by Paul [13]. From [49].

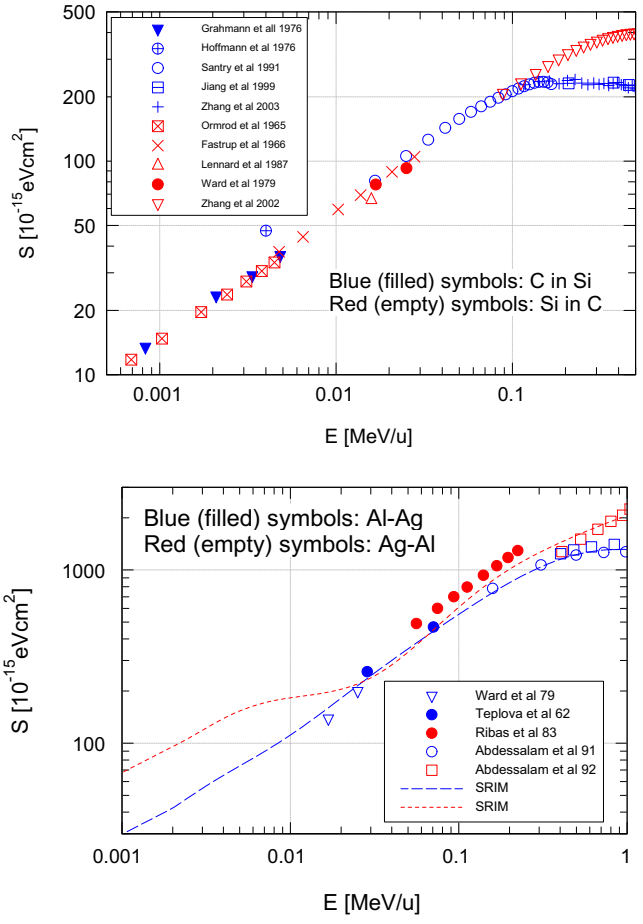

Fig. 13. Same as Fig. 12 for C–Si and Si–C (upper graph) and Ag–Al and Al–Ag (lower graph). Experimental data compiled by Paul [13]. From [49].

This quantity is independent of the frame of reference from which it is measured. If no electrons are emitted, the quantity $S(v)$ must represent the stopping cross section, regardless of whether 1 is the projectile and 2 the target or vice versa, i.e.,

$$S_{12}(v) = S_{21}(v). \tag{11}$$

Fig. 12 shows two typical examples. In either case one may identify a straight line containing experimental data for both S_{12} and S_{21}, whereas one data set may be identified that falls outside. In the upper graph, data by Price et al. [50] appear higher, although this is in the velocity range above v_0. In the lower graph, data by Fukuda [51] fall clearly outside, presumably because of an incorrect nuclear-stopping correction [49].

Fig. 13 demonstrates the use of the reciprocity principle for solid targets. While one may argue that the good agreement between data for Si–C and C–Si might be fortuitous since carbon and silicon are somewhat similar, a study of a wide variety of ion-target combinations has supported the usefulness of the principle also for other materials [49].

The lower graph in Fig. 13 illustrates that the widely used SRIM code [52] claims the stopping cross section of Ag in Al to be more than twice that of Al in Ag at energies corresponding to velocities up to $\sim 0.1\,v_{TF}$. This claim is not supported by stopping measurements. Electronic stopping cross sections for low-energy heavy ions may be extracted from range measurements, but because of the dominance of nuclear stopping, a small error in the adopted nuclear stopping cross section may cause a significant error in the extracted electronic stopping cross section.

It was concluded in Ref. [49] that the reciprocity principle may be a tool

- to check the validity of experimental data,
- to estimate missing data and
- to check semi-empirical tabulations.

We emphasize that reciprocity in electron stopping refers to the stopping cross section versus velocity or energy/nucleon, while reciprocity in nuclear stopping refers to the stopping cross section versus energy in the center-of-mass frame.

The reciprocity principle implies that the well-documented Z_1 structure must mirror an equivalent Z_2 structure [49]. Due to a shortage of experimental data this assertion has not been either confirmed or rejected so far. With a new computational tool, the REST code [53], this aspect as well as several others are being studied in greater detail.

7. Charge equilibrium

Early applications of the PASS code [26,54] focused on ions up to argon. Calculations of stopping cross sections on the basis of several adopted expressions for the equilibrium charge indicated only minor variations. As is evident from Fig. 9, stopping cross sections for heavier ions depend more sensitively on the adopted charge-state function.

We have studied equilibrium charge states for some time, and reference has been made in [25] to unpublished results which

Please cite this article in press as: P. Sigmund, A. Schinner, Progress in understanding heavy-ion stopping, Nucl. Instr. Meth. B (2015), http://dx.doi.org/10.1016/j.nimb.2015.12.041

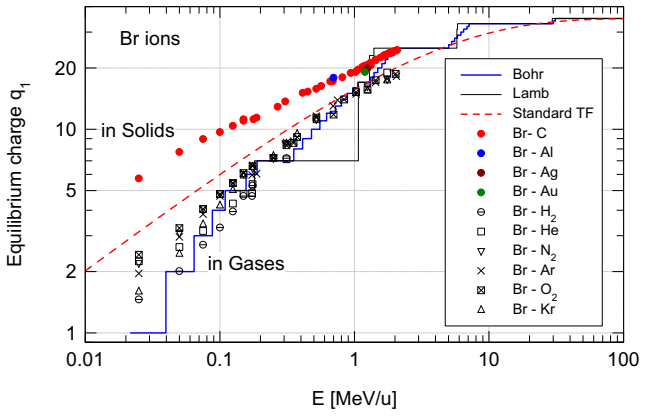

Fig. 14. Equilibrium charge states for Br ions in solids and gases. Experimental values compiled by Schiwietz & Grande [45]. See text. From [25].

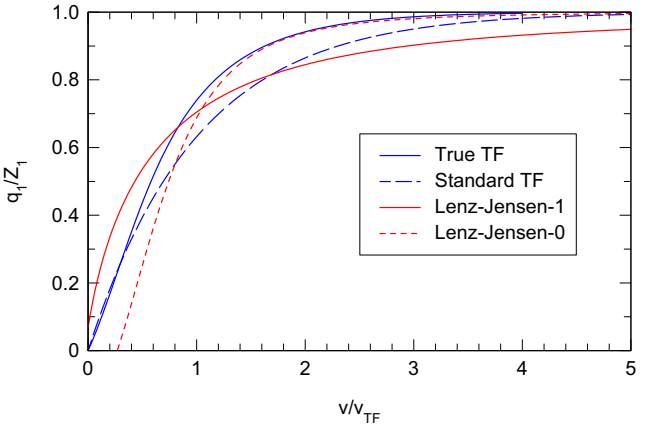

Fig. 15. Universal expressions for the mean equilibrium charge based on Lamb's model. See text. From [25].

we expected to be submitted to a journal shortly. Although our studies of this area continue, we find it appropriate to report some results with relevance to the scope of the present paper.

Early estimates of equilibrium charges date back to Lamb [55] and Bohr [56]. Lamb's criterion claims the total energy of an atom in motion,

$$\mathcal{E} = E(q_1) + N_1 m v^2/2 \tag{12}$$

to be minimal in charge equilibrium. Here, $E(q_1)$ is the total energy of an atom at rest and $N_1 = Z_1 - q_1$ the number of electrons bound to the atom. Bohr's criterion claims that in charge equilibrium, electrons with orbital velocities v_e lower than the projectile speed v are stripped.

Fig. 14 shows a comparison with measured charge states for Br ions. Note that neither Bohr's nor Lamb's criterion involves properties of the target. Bohr's criterion has been implemented by requiring that electrons with

$$\langle v_{n\ell}^2 \rangle < v^2 \tag{13}$$

are stripped, where $v_{n\ell}$ is the orbital speed of an electron in the $n\ell$-shell, calculated from Clementi wave functions [57]. Lamb's criterion was implemented on the basis of tabulated shell binding energies. As is to be expected from the underlying physical picture, the two criteria lead to rather similar results. In the graph, the Bohr model reveals a finer staircase structure since $\langle v_{n\ell}^2 \rangle$ was evaluated for each charge state. Lamb's criterion shows broad plateaus [58] at the transitions between shells.

It is seen that the Bohr criterion leads to good agreement with measurements for gases from ~0.1 MeV/u upward, while charge states measured for solids are significantly higher according to the well-known gas–solid effect [59]. The standard Thomas–Fermi charge (8) is found to lie close to the average between the two groups of data. Similar conclusions have been found for iodine ions as reported in [25].

In the original paper [55], Lamb evaluated a universal expression for the equilibrium charge on the basis of the Thomas–Fermi model of the atom. We reproduced Lamb's result as well as a subsequent evaluation in Ref. [60]. Fig. 15 compares this curve (labeled 'True TF') with the standard Thomas–Fermi charge (8), which predicts a slightly slower approach to complete stripping. Also included are evaluations of the Lamb criterion on the basis of zero- and first-order Lenz–Jensen densities [61,62]. The Lenz–Jensen model operates on the basis of the Thomas–Fermi energy but with trial functions with an asymptotic behavior different from the true Thomas–Fermi function. According to common experience [63] these densities come closer to Hartree–Fock densities than true Thomas–Fermi densities.

Fig. 15 shows that the zero-order Lenz–Jensen function closely approximates the true Thomas–Fermi function for $v/v_{TF} \gtrsim 1.5$ but predicts a negative equilibrium charge at the low-v end. Conversely, the first-order Lenz–Jensen function predicts an even slower approach toward $q_1 = Z_1$ at high speeds and a small positive charge at $v = 0$. While none of these curves approximates the entire range of experimental data in Fig. 14, we find that in this system the standard Thomas–Fermi charge shows the smallest differences from the data.

The question of the sign of the equilibrium charge at $v = 0$ has been quantified in Ref. [25]. If the electron density of the ion is written as

$$\rho(r) = \frac{N_1}{a} f(r/a), \tag{14}$$

where N_1 is the number of bound electrons, $f(r/a)$ a screening function with the screening radius a, the equilibrium charge is negative at $v = 0$ if

$$\int_0^\infty 4\pi\xi\, d\xi f(\xi) > 7 \int_0^\infty 4\pi\xi\, d\xi f(\xi) \int_0^\xi 4\pi\xi'^2\, d\xi' f(\xi'), \tag{15}$$

where the term on the left represents the electron energy in the Coulomb field of the nucleus and the one on the right the electron–electron energy.

Fig. 16 shows corresponding results where Lenz–Jensen densities have been replaced by Yukawa-type densities. The curve labeled 'Yukawa' was found from the Thomas–Fermi functional with the charge state and the screening radius as variational parameters. It is seen that this predicts an unrealistically high equilibrium charge at $v = 0$. The curve labeled 'Brandt–Kitagawa' is found by the procedure proposed in Ref. [64]. In order to force the equilibrium charge to approach zero at $v = 0$, these authors reduced the electron–electron energy in the Thomas–Fermi functional by a factor 4/7. This was argued to account for the effect of exchange and correlation. The exchange correction – which does not obey Thomas–Fermi scaling – has been added in the graph for the case of argon. It is seen that this correction, indicated by the stippled curve, is far too small to justify such a drastic change. The correlation correction has the opposite sign of the exchange correction.

The screening function of Brandt & Kitagawa has been widely used in the literature. Although the resulting equilibrium charge is in reasonable agreement with other Thomas–Fermi-like estimates, we question the validity of its physical basis and,

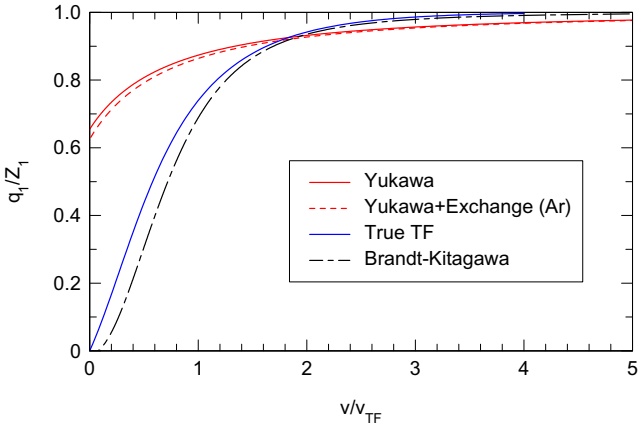

Fig. 16. Same as Fig. 15 for three Yukawa-type charge densities. See text. From [25].

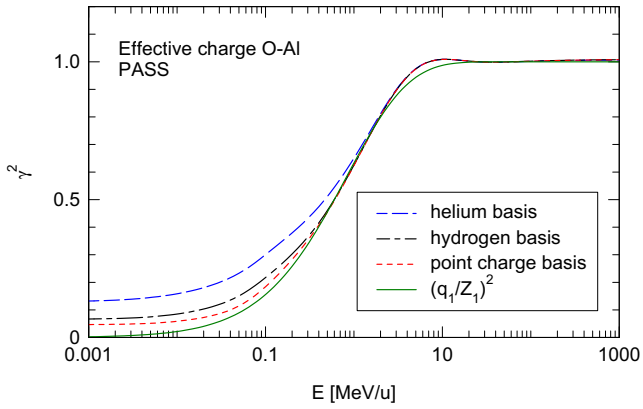

Fig. A.18. Effective-charge ratio γ^2 determined by the PASS code with stopping cross section for a point charge Z_1e as well as dressed ions with a charge q_1e, compared with $(q_1/Z_1)^2$.

hence the applicability of the resulting screening radius in other areas.

8. Summary

1. Well-known dramatic deviations from measured stopping forces are to be expected whenever the Bethe formula is applied outside the range of validity of the Born approximation.
2. In contrast to Northcliffe's assertion, the limit of validity of the Born approximation is found to be determined by the nuclear charge Z_1e as found by Bohr, rather than the ion charge q_1e.
3. The rather common assertion that the stopping force on a screened ion should be proportional to q_1^2 is not confirmed in general. This holds both in the Bethe and the Bohr regime.
4. The so-called effective charge is not a charge. The effective-charge concept is shown to be ambiguous, since normalization to the stopping cross section of a point charge, of a proton or a helium ion yield quite different results.
5. The main cause of the decrease of the effective-charge ratio with decreasing projectile speed is the transition from the Bethe to the Bohr regime, while projectile screening plays a secondary role.
6. The regime of pronounced projectile screening by bound electrons lies outside the range of validity of the Born approximation.
7. We consider four theoretical schemes predicting stopping cross sections. All of them have produced results that compare favorably with experiment. Weaknesses of the CasP code at energies below 1 MeV/u are asserted to originate primarily in the shell correction. This includes the absence of a shell correction to the Barkas–Andersen term.
8. The claim by Lifschitz and Arista that an apparent threshold in the stopping cross sections of Br, I and U ions in carbon does not represent a real threshold but a positive curvature at low energies is confirmed. However, a sudden and unexpected step in the velocity dependence predicted by the TCS-EFSR scheme is not supported by experimental data.
9. The observed curvature may be positive or negative and is found to be determined by a balance between energy lost to target and projectile, respectively. Positive curvature

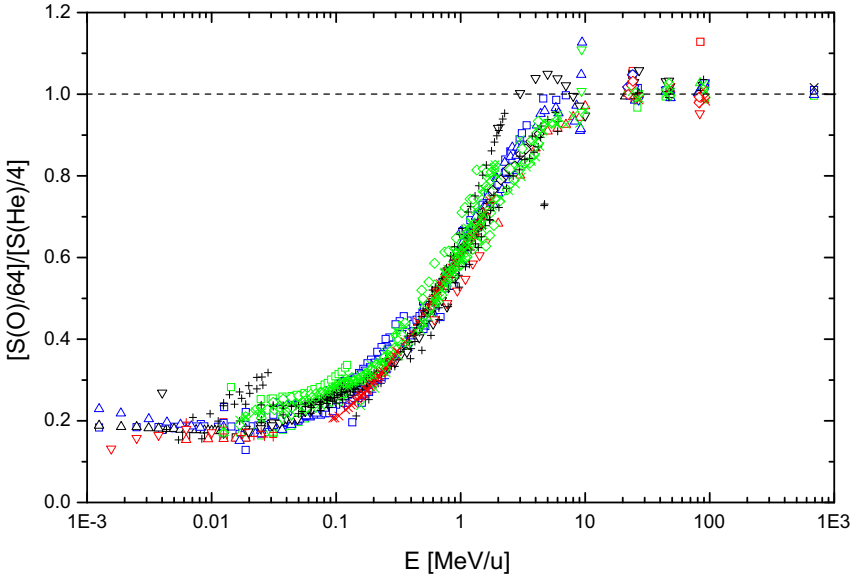

Fig. A.17. γ^2 extracted from measured stopping cross sections for oxygen and helium ions in several materials [13].

Please cite this article in press as: P. Sigmund, A. Schinner, Progress in understanding heavy-ion stopping, Nucl. Instr. Meth. B (2015), http://dx.doi.org/10.1016/j.nimb.2015.12.041

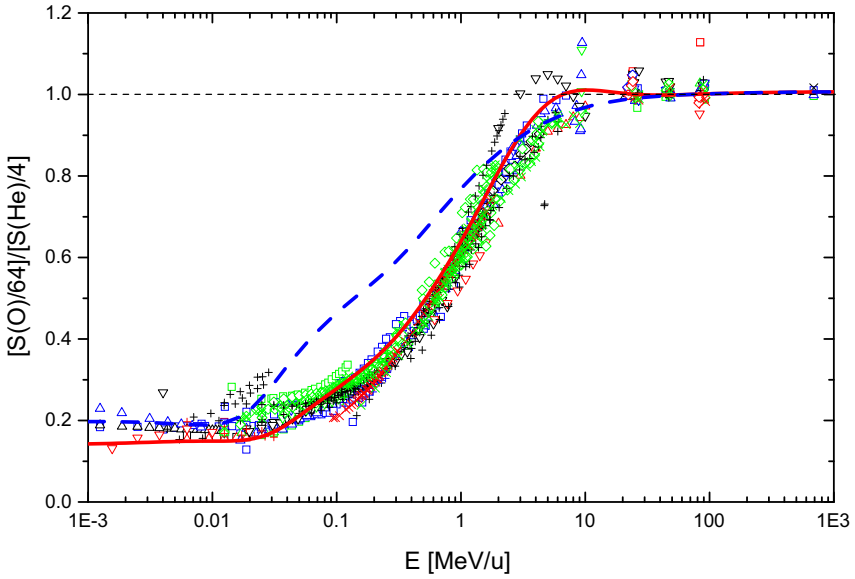

Fig. A.19. Effect of projectile screening on the effective charge. Experimental data from [13] are based on He as the reference ion. Solid line: PASS output for He as reference ion in Fig. A.18. The dashed line represents γ^2 for bare oxygen in aluminum calculated by PASS.

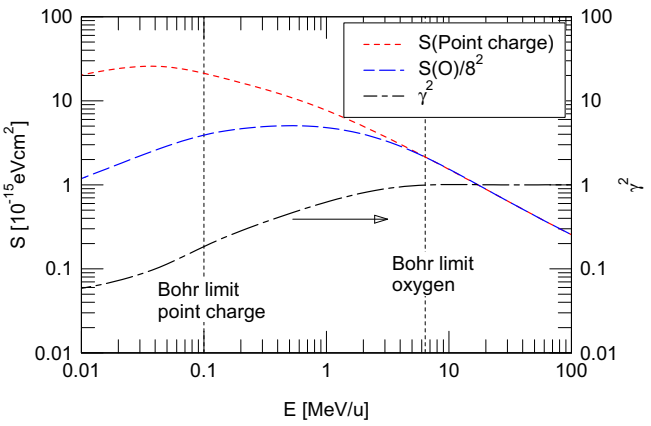

Fig. A.20. Illustration of effective-charge behavior. See text. Dotted curve: $S(8,v)/8^2$; stippled curve: $S(1,v)$; dot-dashed curve: γ^2. Calculated by PASS.

is found to be caused primarily by an increasing occupation of higher charge states. At the same time this decreases the contribution of projectile excitation to the energy loss.

10. As long as there does not exist a comprehensive theory of stopping in the velocity range below the Bohr speed, reciprocity, i.e., comparison of the electronic stopping cross sections for species 1 in species 2 with those for species 2 in species 1, is a useful tool in checking the validity of measured and/or tabulated data as well as estimating stopping cross sections in cases where only one of the two values is available.
11. Estimates of equilibrium charges on the basis of Bohr's or Lamb's criteria yield acceptable results for gas targets at not too low projectile speeds.
12. We have applied Lamb's criterion to estimate equilibrium charges within Thomas–Fermi theory. A variational treatment utilizing the Lenz–Jensen trial function yields a result compatible with the exact Thomas–Fermi charge function in the first order, while the zero-order Lenz–Jensen function leads to a negative equilibrium charge at low velocities.
13. A variational treatment employing a Yukawa-type density leads to a high positive equilibrium charge at $v = 0$. We cannot accept the argument by Brandt and Kitagawa to overcome this problem by reducing the Coulomb energy by a factor 4/7.
14. The widely-used SRIM code [52] combines the scheme of Brandt and Kitagawa with the effective-charge model and an empirical screening radius. SRIM output comes normally close to experimental data where such data exist. As demonstrated in Fig. 13, the credibility of SRIM predictions may decrease dramatically in regions of the (Z_1, Z_2, E) parameter space that is unsupported by experimental data.

Acknowledgement

Thanks are due to G. Schiwietz and P.L. Grande for making their compilation of measured equilibrium charge states available to us. H. Paul's compilation of stopping data has been particularly useful in this project. Special thanks are due to our two referees for thoughtful comments and attentive reading. This work has been supported by the Carlsberg Foundation.

Appendix A. Failure of the effective-charge concept

According to Fig. 1, the Bethe formula dramatically overestimates the stopping force in the interval from ~0.1 to ~2 MeV/u for the system under consideration. This feature has been ascribed to the screening of the ion by bound electrons and characterized by an 'effective charge'. Bohr [56] introduced this concept into classical stopping theory [10], but in all subsequent development the Bethe formula formed the basis [33].

Unlike Bohr theory, Bethe theory predicts a strict Z_1^2 dependence of the stopping cross section according to (1). Within the effective-charge postulate, the stopping cross section $S = (1/N)dE/dx$ can then expressed by

$$S(Z_1, v) = (\gamma Z_1)^2 S(1, v), \tag{16}$$

where the 'effective-charge ratio' γ^2 depends primarily on the projectile speed v and the atomic number of the ion Z_1, and to some

extent on Z_2. In principle, $S(1, v)$ ought to be the stopping cross section of a point charge e. In practice, tabulated cross sections for hydrogen or helium ions in charge equilibrium have been applied [65–67].

Fig. A.17 shows a plot of effective charges of oxygen ions based on helium stopping cross sections tabulated in Ref. [68] and compiled by Paul [13]. It is seen that within a generous margin, the variation with Z_2 in the stopping cross section has been reduced to below ±50% in this plot.

Fig. A.18 shows γ^2 for O in Al calculated by PASS for three choices of the normalizing stopping cross section $S(1)$, compared to the charge ratio $(q_1/Z_1)^2$ according to (8) which enters the PASS calculation of the stopping cross section in this graph. It is seen that γ^2 depends significantly on the choice of $S(1, v)$ for $E < 1$ MeV/u for the O–Al system, and that this difference approaches a factor of ~2 for $E < 0.1$ MeV/u.

Fig. A.19 shows that γ^2 for O–Al, calculated by PASS with He as a basis, is in excellent agreement with the data shown in Fig. A.17. However, we have also included a dashed curve which represents the ratio $S(8, v)/S(2, v)(2/8)^2$, where both the numerator and the denominator represent *bare ions*. This implies that the effect of projectile screening on the effective-charge ratio is represented by the difference between the dashed and the solid curve.[4]

Why, then, does the dashed curve in Fig. A.19 go below $\gamma^2 \equiv 1$, the value expected according to the Bethe formula? Evidently this is caused by the transition from Bethe to Bohr stopping. Fig. A.20 illustrates that this transition is determined by Eq. (2) which depends on Z_1. Starting from high speed, $S(8, v)$ decreases below the Bethe value around 6.4 MeV/u, while $S(1, v)$ follows the Bethe curve until around 0.1 MeV/u. Further on, neither of the two stopping cross sections is proportional to Z_1^2. Therefore, a constant value cannot be expected to be reached. A close look at Fig. A.17 confirms that individual data sets shown in this graph are far from constant in the low-velocity range.

References

[1] N. Bohr, Phys. Rev. 58 (1940) 654.
[2] P.H. Rose, K.H. Purser, A. Wittkower, IEEE Trans. Nucl. Sci. NS12 (1965) 251.
[3] S. Datz, T.S. Noggle, C.D. Moak, Nucl. Instr. Meth. 38 (1965) 221.
[4] J.A. Davies, J.D. McIntyre, R.L. Cushing, M. Lounsbury, Can. J. Chem. 38 (1960) 1535.
[5] W.J. King, S.J. Solomon, J. Electrochem. Soc. 109 (1962) C68.
[6] S. Rubin, Nucl. Instr. Meth. 5 (1959) 177.
[7] J. L'Ecuyer, C. Brassard, C. Cardinal, J. Chabbal, L. Deschenes, J.P. Labrie, B. Tereault, J.G. Martel, R.S. Jacques, J. Appl. Phys. 47 (1976) 381.
[8] C.A. Tobias, J.T. Lyman, J.H. Lawrence, Prog. Atomic Med. 3 (1971) 167.
[9] H. Bethe, Ann. Phys. 5 (1930) 324.
[10] N. Bohr, Philos. Mag. 25 (1913) 10.
[11] N. Bohr, Mat. Fys. Medd. Dan. Vid. Selsk. 18 (8) (1948) 1.
[12] P. Sigmund, Phys. Rev. A 54 (1996) 3113.
[13] H. Paul, Stopping power graphs (2013), <https://www-nds.iaea.org/stopping/>.
[14] A. Schinner, P. Sigmund, Nucl. Instr. Meth. B 164–165 (2000) 220.
[15] C. Vockenhuber, J. Jensen, J. Julin, H. Kettunen, M. Laitinen, M. Rossi, T. Sajavaara, O. Osmani, A. Schinner, P. Sigmund, H.J. Whitlow, Eur. Phys. J. D 67 (2013) 145.
[16] P. Sigmund, O. Osmani, A. Schinner, Nucl. Instr. Meth. B 338 (2014) 101.
[17] J.C. Ashley, R.H. Ritchie, W. Brandt, Phys. Rev. B 5 (1972) 2393.
[18] J. Lindhard, Nucl. Instr. Meth. 132 (1976) 1.
[19] F. Bloch, Z. Phys. 81 (1933) 363.
[20] P. Sigmund, A. Schinner, Eur. Phys. J. D 12 (2000) 425.
[21] G. Schiwietz, P.L. Grande, Nucl. Instr. Meth. B 153 (1999) 1.
[22] N.R. Arista, Nucl. Instr. Meth. B 195 (2002) 91.
[23] C.C. Montanari, J.E. Miraglia, M. Behar, P.F. Duarte, N.R. Arista, J.C. Eckardt, G.H. Lantschner, Phys. Rev. A 77 (2008) 042901.
[24] P. Sigmund, A. Schinner, Nucl. Instr. Meth. B 174 (2001) 535.
[25] P. Sigmund, Particle Penetration and Radiation Effects, Springer Series in Solid State Sciences, vols. 2, 179, Springer, Heidelberg, 2014.
[26] P. Sigmund, A. Schinner, Nucl. Instr. Meth. B 195 (2002) 64.
[27] E.D. Cantero, C.C. Montanari, M. Behar, R.C. Fadanelli, G.H. Lantschner, J.E. Miraglia, N.R. Arista, Phys. Rev. A 84 (2011).
[28] H. Ogawa, I. Katayama, I. Sugai, Y. Haruyama, M. Saito, K. Yoshida, M. Tosaki, H. Ikegami, Nucl. Instr. Meth. B 82 (1993) 80.
[29] H. Ogawa, I. Katayama, H. Ikegami, Y. Haruyama, A. Aoki, M. Tosaki, F. Fukuzawa, K. Yoshida, I. Sugai, T. Kaneko, Phys. Rev. B 43 (1991) 11370.
[30] C.M. Frey, G. Dollinger, A. Bergmaier, T. Faestermann, P. Maier-Komor, Nucl. Instr. Meth. B 107 (1996) 31.
[31] A. Blazevic, H.G. Bohlen, W. von Oertzen, Nucl. Instr. Meth. B 190 (2002) 64.
[32] P. Sigmund, Phys. Rev. A 56 (1997) 3781.
[33] L.C. Northcliffe, Phys. Rev. 120 (1960) 1744.
[34] A.F. Lifschitz, N.R. Arista, Nucl. Instr. Meth. B 316 (2013) 245.
[35] P. Sigmund, A. Schinner, Nucl. Instr. Meth. B 342 (2015) 292.
[36] J. Lindhard, M. Scharff, Phys. Rev. 124 (1961) 128.
[37] J. Lindhard, M. Scharff, H.E. Schitt, Mat. Fys. Medd. Dan. Vid. Selsk. 33 (14) (1963) 1.
[38] B. Fastrup, P. Hvelplund, C.A. Sautter, Mat. Fys. Medd. Dan. Vid. Selsk. 35 (10) (1966) 1.
[39] M.D. Brown, C.D. Moak, Phys. Rev. B 6 (1972) 90.
[40] C.D. Moak, M.D. Brown, Phys. Rev. 149 (1966) 244.
[41] P. Hvelplund, Besvarelse af Aarhus Universitets prisopgave i fysik for aaret 1968, Institute of Physics, Aarhus, 1968.
[42] J.M. Anthony, W.A. Lanford, Phys. Rev. A 25 (1982) 1868.
[43] Y.W. Zhang, G. Possnert, Nucl. Instr. Meth. B 190 (2002) 69.
[44] K. Shima, N. Kuno, M. Yamanouchi, H. Tawara, Atom. Data Nucl. Data Table 51 (1992) 173.
[45] G. Schiwietz, P.L. Grande, Nucl. Instr. Meth. B 175–177 (2001) 125.
[46] P. Sigmund, Izv. Russ. Akad. NAUK Ser. Fiz. 72 (2008) 608 (Bulletin Russ. Acad. Sci. Phys. Ser. 72, 569 (2008)).
[47] O.B. Firsov, Zh. Eksp. Teor. Fiz. 36 (1959) 1517 (Engl. transl. Sov. Phys. JETP 9, 1076–1080 (1959)).
[48] P.M. Echenique, R.M. Nieminen, J.C. Ashley, R.H. Ritchie, Phys. Rev. A 33 (1986) 897.
[49] P. Sigmund, Eur. Phys. J. D 47 (2008) 45.
[50] J.L. Price, D.G. Simons, S.H. Stern, D.J. Land, N.A. Guardala, J.G. Brennan, M.F. Stumborg, Phys. Rev. A 47 (1993) 2913.
[51] A. Fukuda, J. Phys. B 29 (1996) 3717.
[52] J.F. Ziegler, Particle interactions with matter (2012), <www.srim.org>.
[53] V. Kuzmin, P. Sigmund, Nucl. Instr. Meth. B 269 (2011) 817.
[54] ICRU, Stopping of Ions Heavier than Helium, ICRU Report, vol. 73, Oxford University Press, Oxford, 2005.
[55] W.E. Lamb, Phys. Rev. 58 (1940) 696.
[56] N. Bohr, Phys. Rev. 59 (1941) 270.
[57] E. Clementi, C. Roetti, Atomic Data Nucl. Data Tables 14 (1974) 177.
[58] R.J. Mathar, M. Posselt, Phys. Rev. B 51 (1995) 107.
[59] N.O. Lassen, Mat. Fys. Medd. Dan. Vid. Selsk. 26 (5) (1951) 1.
[60] V.N. Neelavathi, R.H. Ritchie, W. Brandt, Phys. Rev. Lett. 33 (1974) 302.
[61] W. Lenz, Z. Phys. 77 (1932) 713.
[62] H. Jensen, Z. Phys. 77 (1932) 722.
[63] P. Gombas, Die Statistische Theorie des Atoms, Springer, Vienna, 1949.
[64] W. Brandt, M. Kitagawa, Phys. Rev. B 25 (1982) 5631.
[65] L.C. Northcliffe, R.F. Schilling, Nucl. Data Tables A 7 (1970) 233.
[66] J.F. Ziegler, J.P. Biersack, U. Littmark, The Stopping and Range of Ions in Solids, The Stopping and Ranges of Ions in Matter, vol. 1, Pergamon, New York, 1985.
[67] H. Paul, A. Schinner, Nucl. Instr. Meth. B 179 (2001) 299.
[68] ICRU, Stopping powers and ranges for protons and alpha particles, vol. 49 of ICRU Report (International Commission of Radiation Units and Measurements, Bethesda, Maryland, 1993).

[4] The fact that this difference becomes negative from ~3 to 30 MeV/u is due to projectile excitation, which is included in the calculations. This is also asserted to be the reason for a similar hump in the experimental data.

Please cite this article in press as: P. Sigmund, A. Schinner, Progress in understanding heavy-ion stopping, Nucl. Instr. Meth. B (2015), http://dx.doi.org/10.1016/j.nimb.2015.12.041